INTERFACE

royalsocietypublishing.org/journal/rsif

Research

Cite this article: Jackson T *et al*. 2019 An architectural understanding of natural sway frequencies in trees. *J. R. Soc. Interface* **16**: 20190116.
http://dx.doi.org/10.1098/rsif.2019.0116

Received: 22 February 2019
Accepted: 13 May 2019

Subject Category:
Life Sciences–Physics interface

Subject Areas:
biophysics, environmental science, biomechanics

Keywords:
natural frequencies, fundamental frequency, tree architecture, terrestrial laser scanning, finite-element analysis, wind damage

Author for correspondence:
T. Jackson
e-mail: tobydjackson@gmail.com

Electronic supplementary material is available online at http://dx.doi.org/10.6084/m9.figshare.c.4510532.

THE ROYAL SOCIETY PUBLISHING

An architectural understanding of natural sway frequencies in trees

T. Jackson[1], A. Shenkin[1], J. Moore[2], A. Bunce[3], T. van Emmerik[4,5], B. Kane[6], D. Burcham[7], K. James[8], J. Selker[9], K. Calders[10], N. Origo[11,12], M. Disney[12,13], A. Burt[12], P. Wilkes[12,13], P. Raumonen[14], J. Gonzalez de Tanago Menaca[15,16], A. Lau[15,16], M. Herold[15], R. C. Goodman[17], T. Fourcaud[18] and Y. Malhi[1]

[1]Environmental Change Institute, School of Geography and the Environment, University of Oxford, Oxford OX1 3QY, UK
[2]Scion, 49 Sala Street, Rotorua 3010, New Zealand
[3]Department of Natural Resources, University of Connecticut, Mansfield, CT 06269, USA
[4]Water Resources Section, Delft University of Technology, Stevinweg 1, 2628 CN, Delft, The Netherlands
[5]Hydrology and Quantitative Water Management Group, Wageningen University, Wageningen, The Netherlands
[6]Department of Environmental Conservation, University of Massachusetts, Amherst, MA 01003, USA
[7]Centre for Urban Greenery and Ecology, National Parks Board, 259569 Singapore
[8]School of Ecosystem and Forest Sciences, Faculty of Science, University of Melbourne, Melbourne, Australia
[9]Oregon State University, Corvallis, OR 97331, USA
[10]CAVElab - Computational and Applied Vegetation Ecology, Ghent University, Ghent, Belgium
[11]Earth Observation, Climate and Optical Group, National Physical Laboratory, Hampton Road, Teddington, Middlesex TW11 0LW, UK
[12]Department of Geography, University College London, London WC1E 6BT, UK
[13]NERC National Centre for Earth Observation (NCEO), Leicester, UK
[14]Tampere University of Technology, Korkeakoulunkatu 10, 33720 Tampere, Finland
[15]Laboratory of Geo-Information Science and Remote Sensing, Wageningen University, Droevendaalsesteeg 3, 6708 PB Wageningen, The Netherlands
[16]Center for International Forestry Research (CIFOR), PO Box 0113 BOCBD, Bogor 16000, Indonesia
[17]Department of Forest Ecology and Management, Swedish University of Agricultural Sciences, Umeå, Sweden
[18]AMAP, University of Montpellier, CIRAD, CNRS, INRA, IRD, Montpellier, France

TJ, 0000-0001-8143-6161; AS, 0000-0003-2358-9367; MD, 0000-0002-2407-4026; YM, 0000-0002-3503-4783

The relationship between form and function in trees is the subject of a long-standing debate in forest ecology and provides the basis for theories concerning forest ecosystem structure and metabolism. Trees interact with the wind in a dynamic manner and exhibit natural sway frequencies and damping processes that are important in understanding wind damage. Tree-wind dynamics are related to tree architecture, but this relationship is not well understood. We present a comprehensive view of natural sway frequencies in trees by compiling a dataset of field measurement spanning conifers and broadleaves, tropical and temperate forests. The field data show that a cantilever beam approximation adequately predicts the fundamental frequency of conifers, but not that of broadleaf trees. We also use structurally detailed tree dynamics simulations to test fundamental assumptions underpinning models of natural frequencies in trees. We model the dynamic properties of greater than 1000 trees using a finite-element approach based on accurate three-dimensional model trees derived from terrestrial laser scanning data. We show that (1) residual variation, the variation not explained by the cantilever beam approximation, in fundamental frequencies of broadleaf trees is driven by their architecture; (2) slender trees behave like a simple pendulum, with a single natural frequency dominating their motion, which makes them vulnerable to wind damage and (3) the presence of leaves decreases both the fundamental frequency and the damping ratio. These findings demonstrate the value of new three-dimensional measurements for understanding wind impacts on trees and suggest new directions for improving our understanding of tree dynamics from conifer plantations to natural forests.

1. Introduction

1.1. Natural frequencies and tree architecture

The dynamics of trees in the wind has interested observers for centuries, but detailed studies concerning the risk of wind damage are relatively recent [1,2]. All structures that can sway, such as trees in the wind, possess natural frequencies—characteristic shapes and speeds at which the motion is concentrated. The natural frequencies of a tree are related to its architecture [3,4] and they influence its response to wind loading [5], thus linking form and function. However, due to the difficulty of obtaining detailed information on tree architecture, this link has remained largely unexplored (although see [4]). Recently, terrestrial laser scanning (TLS) has revolutionized the mapping of tree architecture [6], paving the way for more detailed studies on this intriguing subject.

The lowest natural frequency, known as the fundamental frequency (f_0), is particularly relevant for wind damage risk. This is because wind energy is concentrated at low frequencies [7] and energy will be transferred from the wind to the tree more efficiently in trees with lower f_0, a phenomenon known as resonance [8–10]. Previous work found that the f_0 of 602 conifers in the UK and North America was accurately predicted by the cantilever beam approximation [8,9], which models the tree as a vertically oriented cylinder with uniform radius and material properties. According to this approximation, f_0 will decrease with increasing tree height, leading to an increased likelihood of resonant effects in taller trees. Importantly, no field study has yet recorded the moment a tree breaks or uproots due to wind loading [11] and the relevance of resonant effects in wind damage is the subject of ongoing debate in the literature [11–14].

Knowledge about the natural frequencies of a structure allows for a detailed model of that structure's dynamics under loading. In the case of conifer trees in the wind, data on f_0 provided the basis for an accurate model of tree motion under wind loading at the plot level [15]. This was possible because the dynamics of conifers are, in uniform plantations, dominated by f_0 due to their simple architecture. However, the dynamic properties of broadleaf trees are unlikely to follow these simple patterns, but rather consist of multiple significant natural frequencies and be dependent on tree architecture and the presence or the absence of leaves [3,16]. Trees with multiple significant natural modes can exhibit multiple resonance damping, a dynamic process whereby dangerous energy in the stem is dissipated by the movement of the branches [17,18]. The existence of this damping mechanism demonstrates the relationship between wind damage risk and tree architecture: trees with certain architectures will dissipate dangerous sway energy more efficiently and so reduce their risk of damage in storms. See Spatz & Theckes [17] for a review of multiple resonance damping (and the similar concepts of structural damping and damping by branching).

1.2. Objectives and structure of the paper

Our overall aim is to explore the relationship between tree architecture and the dynamics of trees in the wind, in particular their natural sway frequencies. We employ the cantilever beam approximation (equation (1.1)), appropriate to the simple architecture of many conifers, as a starting point and add additional terms to explain residual variation caused by the complexities of broadleaf trees (equation (1.1)). Our updated equation takes the form:

$$f_0 \propto \left(\frac{\mathrm{dbh}}{H^2}\sqrt{\frac{E}{\rho}}\right) A \times L, \tag{1.1}$$

where H is tree height and dbh is the diameter at breast height, measured at 1.3 m, and E/ρ is the ratio of green wood elasticity to density. The additional terms A and L represent the effect of tree architecture and leaves, as described below. In order to explore these additional terms, we:

(1) Collate field data on f_0 for 163 broadleaf trees spanning open-grown conditions, tropical forests, temperate forests and a height range of 4.7–55.7 m (see electronic supplementary material, table S1 for a detailed overview). We then use this field data to test the applicability of the cantilever beam approximation to broadleaf trees. Architectural information was not collected in these studies and is immensely difficult to collect in the field.
(2) Explore the range of tree architecture by bringing together TLS data for 1083 trees from previous studies spanning tropical and temperate forests, cities and parks (electronic supplementary material, table S1). We also test for covariance between these architectural indices, since they are used as explanatory variables in the next step.
(3) Quantify the architectural term, A (equation (1.1)) in a model environment. We use finite-element analysis to simulate f_0 (figure 1) for each of the 1083 trees. We then test how well the cantilever beam approximation predicts the simulated f_0 and whether any residual variation can be explained by the architectural indices extracted in the previous step.
(4) Calculate the dominance of the fundamental sway mode, D_0, based on the same finite-element simulations and test how it is related to tree architecture. D_0 is defined as the percentage of generalized mass contained in f_0. Trees with $D_0 > 90\%$ behave like a simple pendulum, with a single dominant sway mode, while lower D_0 values correspond to an increasing significance of higher order natural sway modes in the overall motion of the tree.
(5) Use pull and release data to explore how leaves change f_0 and damping rates in deciduous broadleaf trees.

2. Material and methods

2.1. Analysis of field data

In order to extract field data on f_0, we measured wind-induced strain (extension/original length) following Moore *et al*. [19] for a period of eight months (spanning winter and summer) at 1.3 m height on the trunks of 18 trees (21 stems) in Wytham Woods, UK, and for five months on 20 trees in Danum Valley, Malaysia. We separated the strain data into hourly blocks and analysed them using a Welch's power spectral density function [20]. We smoothed the resulting spectra and extracted the peak frequencies. We then took the mean of all the hourly frequencies. We also collated data on the f_0 of trees from previous studies (see the electronic supplementary material, table S1 for an overview of field data). Fundamental frequency extraction from previous studies are described in the original publications [3,9,21–25].

To investigate the damping effect of leaves, we conducted pull and release tests on four trees (two *Acer pseudoplatanus* L.,

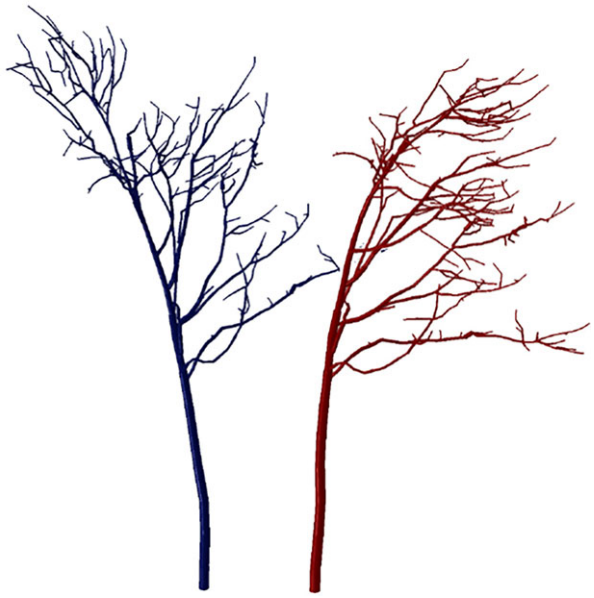

Figure 1. Simulated fundamental sway frequency of a tree. Finite-element simulation output showing the two extreme positions (blue and red) for a sycamore tree (*Acer pseudoplatanus*) swaying at its fundamental frequency, $f_0 = 0.26$ Hz. (Online version in colour.)

one *Fraxinus excelsior* L. and one *Betula* spp.) in Wytham Woods in February 2016 (leaf-off) and June 2016 (full-leaf), repeating the tests multiple times per tree in perpendicular directions. The trees behaved like damped harmonic oscillators and we therefore fit functions of the form

$$\varepsilon = \varepsilon_0 e^{-\lambda t} \cos(2\pi f_0 t + \theta), \tag{2.1}$$

to the data, where ε is strain, ε_0 is the initial strain, λ is the decay exponent, t is time and θ is the phase offset at time $t = 0$. The direct effect of damping on f_0 is given by

$$f_0^d = f_0^u \sqrt{1 - \left(\frac{\lambda}{2\pi f_0^u}\right)^2}, \tag{2.2}$$

where f_0^d and f_0^u are the damped and undamped fundamental frequencies, respectively.

2.2. Terrestrial laser scanning data and tree architectural indices

TLS data contains highly useful information on the three-dimensional structure of trees, but it is difficult to access directly from the point cloud. Therefore, quantitative structure models (QSMs), which are three-dimensional representations of the trees as a series of cylinders, are often fit to the raw TLS data [26]. We brought together 1083 QSMs from existing publications and ongoing projects [27–32]. In all cases, TLS data were collected with a Riegl VZ-400, but sampling details were study specific (see the electronic supplementary material, table S1 for details). We applied a simplification step in order to prepare the QSMs for finite-element analysis. This step removes QSM branches under 2 cm diameter and child branches whose diameter is less than 30% of its parent branch diameter, since they are error prone [33]. It also replaces each pair of neighbouring cylinders with a single cylinder with an increase their length to radius ratio and the mean orientation and radius of the original pair. This simplification was applied to remove most of the variation that arises from uncertainties in the cylinder fitting process for smaller branches. This level of simplification was chosen because the sensitivity of the architectural indices was relatively low (see electronic supplementary material, figures S6 and S7 for details). The following architectural indices, in addition to tree height and dbh, were extracted from the simplified QSMs:

— Crown area—maximum ground area covered by the crown viewed from above. The crown is defined as all the cylinders with branching order greater than one, which is given by the QSM fitting software.
— Crown aspect ratio—ratio of maximum crown width to crown height.
— Crown volume ratio (CVR)—ratio of total woody volume to that in the crown. This is an inverse measure of how 'top-heavy' the tree is.
— Crown volume asymmetry—the ratio of mean to maximum woody volume contained in each segment of crown. These segments were defined starting from the position of the base of the tree and summing the volume of cylinders in the crown between angles 0–45°, 46–90°, etc.
— Path fraction—ratio of mean to maximum base-to-twig path length, this is considered a proxy for water use efficiency [34,35].
— Mean branching angle—the average angle between two cylinders at each branching point.
— Total volume—total volume of all the cylinders that make up the tree.

No validation of these architectural indices was possible since measuring tree architecture in the field is extremely slow and difficult. Indeed, it is exactly this difficulty that has hampered previous studies on tree architecture, which are now possible through TLS [6]. Previous work found that these QSMs are accurate enough to extract architecture information sufficient to identify species in a three-species environment [36]. Importantly, the TLS data quality differs systematically between study sites due to differences in forest structure [33]. Simple architectural indices such as crown area are likely to be robust, but more complex measures such as crown asymmetry may be less accurate in tall dense forests. A validation study of these, and other, TLS-derived architectural indices across different forest types would be highly valuable, albeit extremely time consuming.

2.3. Finite-element analysis

Finite-element analysis is a computational technique capable of simulating the dynamics of complex structures. It is the de facto investigation tool used to isolate mechanisms related to branched structures [11,18,37,38]. The QSMs were imported into Abaqus [39], with each cylinder represented as a beam. First, a gravitational force was applied to the trees, which caused a number of simulation failures due to poorly connected beams. This reduced the sample size from 577 to 568 for the temperate trees, 451 to 348 for the tropical trees and 56 to 52 for the open-grown trees. A subspace method [40] was employed to extract the natural frequencies and D_0 was calculated as the percentage of generalized mass contained in the f_0. This definition was chosen to give an indication of the significance of the fundamental mode in the overall motion of the tree. Other metrics, such as the distribution of modes in frequency space, could be used in future studies. See Jackson *et al.* [41] for a detailed description of the finite-element method applied to QSMs.

Due to the difficulty of co-locating TLS and census data, the species of trees represented by the QSMs were generally not determined in the original studies. Therefore, green wood density and elasticity were kept constant for all simulations at 800 kgm^{-3} and 9.5 GPa, respectively [42]. Our sensitivity analysis (electronic supplementary material, table S3) showed that this uncertainty is unlikely to affect our predictions of f_0. This is in agreement with Sellier & Fourcaud [4] who found that the effect of material properties on tree dynamics is likely to be secondary to that of tree

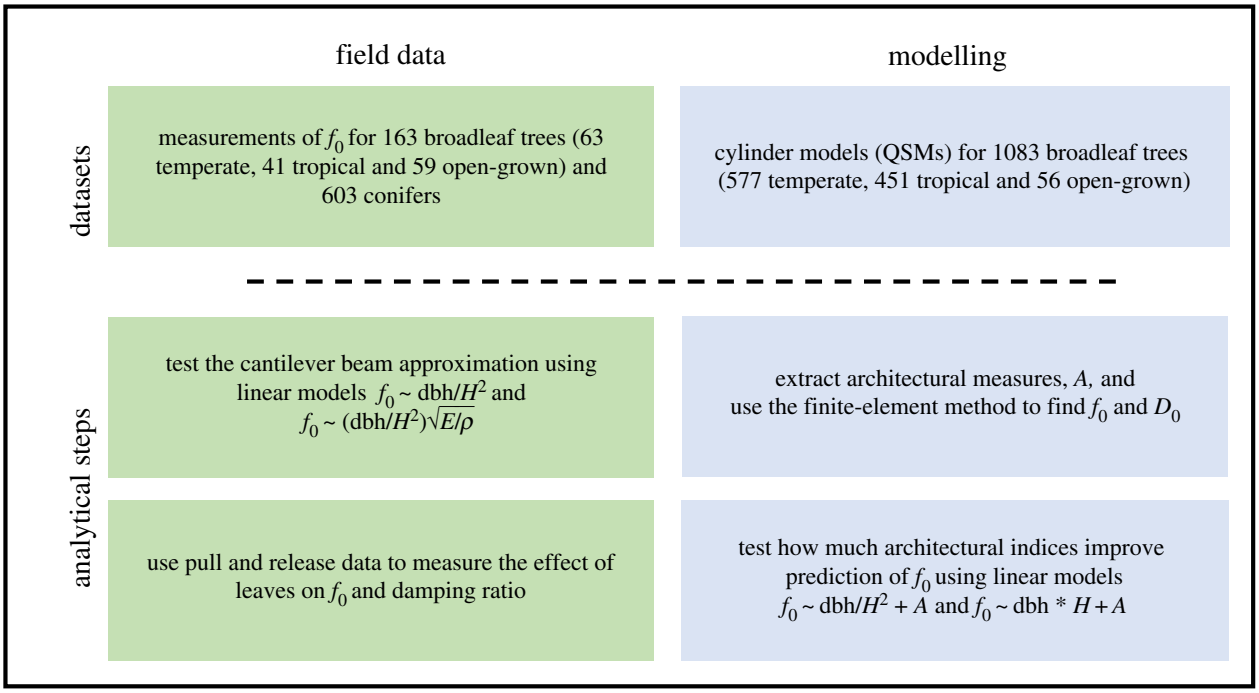

Figure 2. Workflow diagram. (Online version in colour.)

architecture. Importantly, the same simplified model trees were used for the finite-element simulations and to extract the architectural indices, so our linear models predicting f_0 and D_0 from architecture are internally consistent.

2.4. Statistical analysis

For the field data, we tested linear regression models of the form $f_0 = 1 + \mathrm{dbh}/H^2$ for each subset of trees (temperate forest, tropical forest, open-grown and conifer forest). For a subset of 40 broadleaf trees, those for which material properties information was available in Niklas & Spatz [42], we tested a linear model of the form $f_0 = 1 + (\mathrm{dbh}/H^2)\sqrt{E/\rho}$ (this subset is indicated in electronic supplementary material, table S1 and the results are given in electronic supplementary material, table S2).

For the QSMs, for which we had both architectural information and simulated f_0 and D_0, we used linear models of the form $f_0 = 1 + \mathrm{dbh}/H^2 + (A_1 + A_2 + A_3)$ and $f_0 = 1 + \mathrm{dbh}/H^2 + \mathrm{dbh}/H^2$: $(A_1 + A_2 + A_3)$ to predict f_0 for each subset of trees, allowing the intercept to vary between subsets (linear models specified in Wilkinson notation). The same method was used for D_0 except that in this case $H + \mathrm{dbh}$ was the primary predictor variable. We used ordinary least-squares linear regression models for all the statistical analysis in this study. We ensured this method was appropriate by inspecting the residuals and testing robust regressions. The only problematic models were those for the open-grown trees, for which the result was highly dependent on the inclusion of 12 small trees. In these cases, we give both results and our conclusions are necessarily tentative where open-grown trees are concerned. In all cases, we selected the optimal model based on highest predictive power (adjusted R^2) and lowest Akaike information criteria (AIC). See the electronic supplementary material, figures S1–4 for full details of the linear models and their outputs.

An overview of the workflow is given in figure 2.

3. Results

3.1. Patterns in f_0 from field data

In this section, we test the applicability of the cantilever beam approximation to all of the field data on f_0. We find that f_0 is strongly related to dbh/H^2 for conifers, indicating that the cantilever beam approximation is accurate (see table 1 for fit statistics). This relationship is weaker for broadleaf trees (figure 3*a*) presumably due to their more varied architectures. This was expected, since trees with large branches clearly do not conform to the cantilever beam approximation. Differences between tropical and temperate forest broadleaf trees are not statistically robust in this limited sample. For a subset of 40 trees, we found that including material properties actually lowered the adjusted R^2 from 0.33 to 0.31 (see electronic supplementary material, table S2). This lack of explanatory power is likely due to the large range of inter- and intraspecific variation in material properties that is not accounted for in this simplistic approach [14,42]. Surprisingly, f_0 for open-grown broadleaf trees was well predicted by the cantilever beam approximation (table 1), even though these trees typically display the least 'beam-like' architecture. This is partly driven by the large range of f_0 and tree size in our open-grown tree sample. In addition, this high predictability could be due to a smaller range of architectures in open-grown trees.

3.2. Tree architecture

In this section, we explore our seven architectural indices using the TLS-derived QSMs collated from previous studies. Instantly apparent from figure 4 is the large range of architectural variation in the tropical trees, as compared to the temperate or open-grown trees. The primary axis of variation is driven by tree size: total volume, dbh and crown area are closely aligned and they account for much of the separation between the relatively small trees from a temperate forest in the UK and the large tropical trees. The second axis of variation is driven by crown properties, specifically the CVR and crown asymmetry. This suggests that some tropical trees have crowns that are both asymmetric and small relative to their stem, and that this does not occur in the open-grown trees in our sample. Instead, open-grown trees tend to have large, wide crowns and high path fractions. Correlations

Table 1. Summary of linear models for f_0 and D_0. The entries are adjusted R^2-values for ordinary least-squares linear regression models. In the case of f_0, the three architectural indices are CVR, crown asymmetry and aspect ratio. In the case of D_0, the two architectural indices are total tree volume and crown area. The numbers in parentheses for the open-grown trees correspond to the insets in figure 5, they demonstrate the sensitivity of linear models to outliers in this sample.

		field data		model results				
		N	$f_0 \propto \mathrm{dbh}/H^2$	N	$f_0 \propto \mathrm{dbh}/H^2$	$f_0 \propto \mathrm{dbh}/H^2 \times (A_1 + A_2 + A_2)$	$D_0 \propto H + \mathrm{dbh}$	$D_0 \propto H + \mathrm{dbh} + A_1 + A_2$
broadleaf	temperate[a]	63	0.32	568	0.42	0.83	0.09	0.12
	tropical	41	0.09	348	0.16	0.56	0.16	0.29
	open-grown	59	0.45	54 (42)	0.82 (0.18)	0.93 (0.42)	0.29	0.69
conifers		603	0.77	—	—		—	
all trees		765	0.55	970	0.62	0.86	0.26	0.40

[a]For temperate deciduous trees, the field data were measured in full-leaf. All models are specified in Wilkinson notation. For details on linear model selection, see electronic supplementary material, figures S1–S4.

between architectural indices are given in the electronic supplementary material, figure S5 and the sensitivity of these architectural indices to simplification are given in electronic supplementary material, figures S6 and S7.

3.3. The effect of tree architecture on f_0

In this section, we use the 1083 TLS-derived QSMs to simulate f_0 and then test whether it is well modelled by the cantilever beam approximation, and whether the residual variation is driven by architecture. Across all the simulations, linear models showed that dbh/H^2 was positively correlated with f_0 meaning that slender trees tend to have low f_0. As in our field data, this relationship was weakest for the tropical trees (figure 4), presumably due to the higher range of architectures in this sample. The architectural term, A, improves f_0 predictability in all samples (figure 5). The predictability increased by approximately 40% in both temperate and tropical trees (table 1). Trees with large crown volume ratios tended to have lower f_0, while high crown asymmetry and aspect ratio were correlated with higher f_0 (see the electronic supplementary material, figure S2 for effect sizes). In this analysis we used the model with highest predictive power (adjusted R^2) and lowest AIC (see electronic supplementary material, figure S1), which was a three-parameter model focusing on crown architecture. However, all of our architectural indices improved the predictability of f_0 to different extents and the key message is that any architectural information is useful when attempting to predict tree dynamics.

3.4. Dominance of the fundamental sway mode

In this section, we explore the predictability of D_0, the dominance of the fundamental sway mode, based on simulations of the 1083 TLS-derived QSMs. Linear models showed that height and diameter explained 26% of the variation in D_0 across all QSMs (table 1). Taller trees tended to have higher D_0, while a larger dbh was associated with lower D_0 (electronic supplementary material, figure S4). This suggests that slender trees behave more like a simple pendulum, with the fundamental mode accounting for the majority of the motion. Architectural indices did not substantially improve our ability to predict of D_0, accounting for only 14% of the residual variation. Within our small subset of open-grown trees, it was possible to predict D_0 from tree height, dbh and total volume (table 1) but further open-grown tree data would be needed to robustly explore this relationship.

3.5. The effect of leaves

The swaying behaviour of deciduous trees changes as leaves fall in the autumn. We found that the mean f_0 increased by 19.4% in winter in Wytham Woods (figure 6). These changes are nearly uniform and can easily be parametrized. If we define L (equation (1.1)) as the increase of f_0 in winter, then $L = 1.18 \pm 0.12$. We expect that the magnitude of this term will be influenced by total leaf biomass, which varies from site to site. For comparison with other forest plots, the leaf mass per unit ground area in Wytham Woods was measured to be $0.35 \pm 0.02\ \mathrm{kg\,m^{-2}}$ (dry weight) through direct measurement of cumulative autumn litterfall.

Repeated pull and release tests on the same four trees in summer and winter determined the summer damping ratio to be $8.6 \pm 2.2\%$ and the winter damping ratio to be $3.9 \pm$

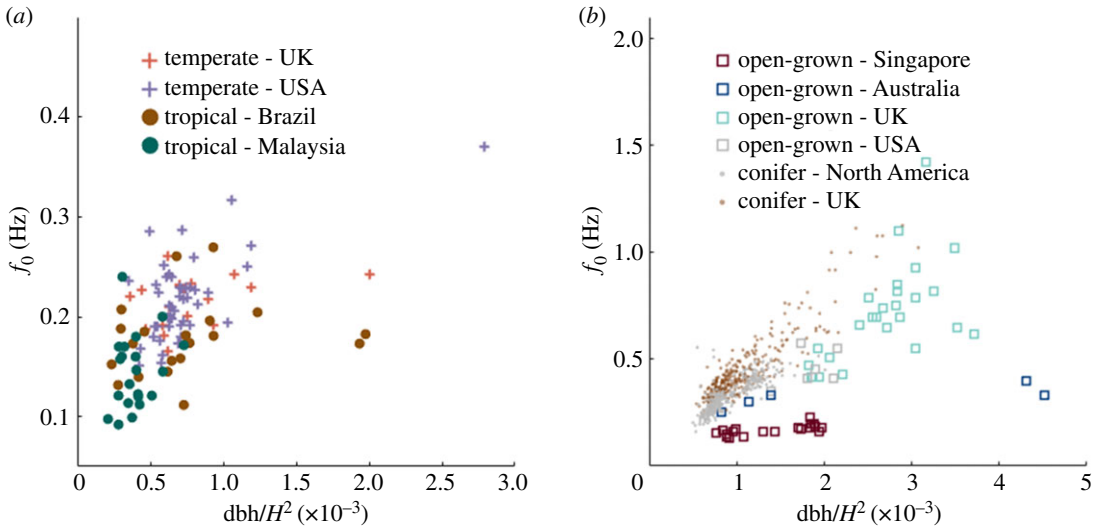

Figure 3. Fundamental frequencies from field data. f_0 against dbh/H^2 for (*a*) broadleaf forest trees from temperate and tropical forests and (*b*) open-grown broadleaf trees and plantation conifers. Note the difference in axis ranges. (Online version in colour.)

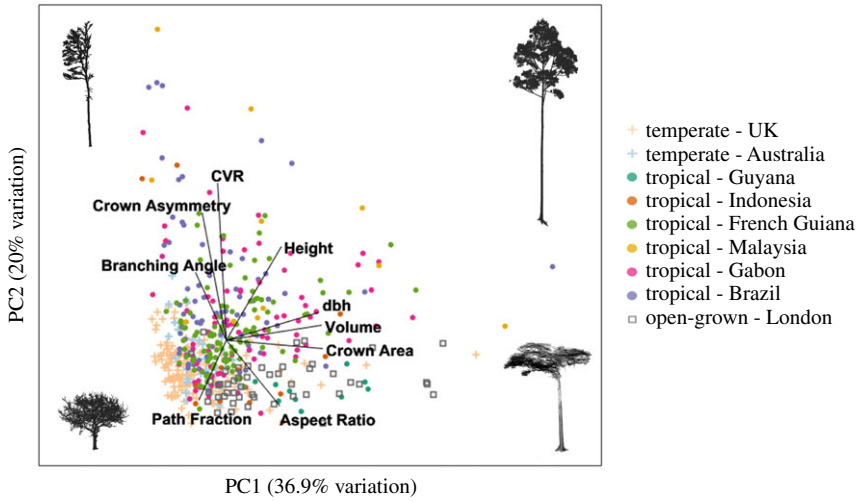

Figure 4. Tree architectural indices. Principal component analysis of the architectural indices extracted from QSMs. Only trees with dbh $>$ 30 cm were included in the analysis for clarity, but this did not substantially change the results. The overlaid images of trees are TLS point clouds which were selected as characteristic examples of the architecture expected at their position in the diagram. (Online version in colour.)

1.3%. If we assume that changes in temperature and air density do not have a significant effect on damping, we find that the leaves contributed a damping ratio $4.7 \pm 2.5\%$ or approximately half the full summer damping ratio. The direct effect of this damping on f_0 is less than 1% (equation (2.2)). This means that the change in f_0 is due to the mass of the leaves, not their aerodynamic drag.

4. Discussion

By using novel tools and sensors, particularly a large number of detailed three-dimensional measurements of individual tree structure across biomes, we have improved our understanding of the dynamic behaviour of broadleaf trees. In particular, we have introduced a new way to quantify the impact of tree architecture on natural frequencies. The improved predictability of f_0 is a step towards mechanistic modelling of wind damage for natural broadleaf forests, which plays a vital role in the terrestrial carbon cycle [43–45].

4.1. Tree architecture

We explored the range of tree architecture across 1083 broadleaf trees from tropical forests, temperate forests, parks and cities using QSMs based on TLS data. The primary axis of variation was driven by tree size and the secondary axis of variation by crown shape (figure 4). Interestingly, open-grown trees tended to cluster around high path fraction, the optimum architecture for hydraulic transport [35], as we would expect in the absence of competition for light or resources. More work is needed to validate these architectural measures and explore their sensitivity to TLS data processing parameters (see electronic supplementary material, figures S6 and S7).

4.2. Beyond the cantilever beam approximation

Most trees in our sample exhibited a clear f_0, which was related to dbh/H^2 as expected from the cantilever beam approximation (equation (1.1)). However, in the case of broadleaf trees, and especially tropical broadleaf trees, there

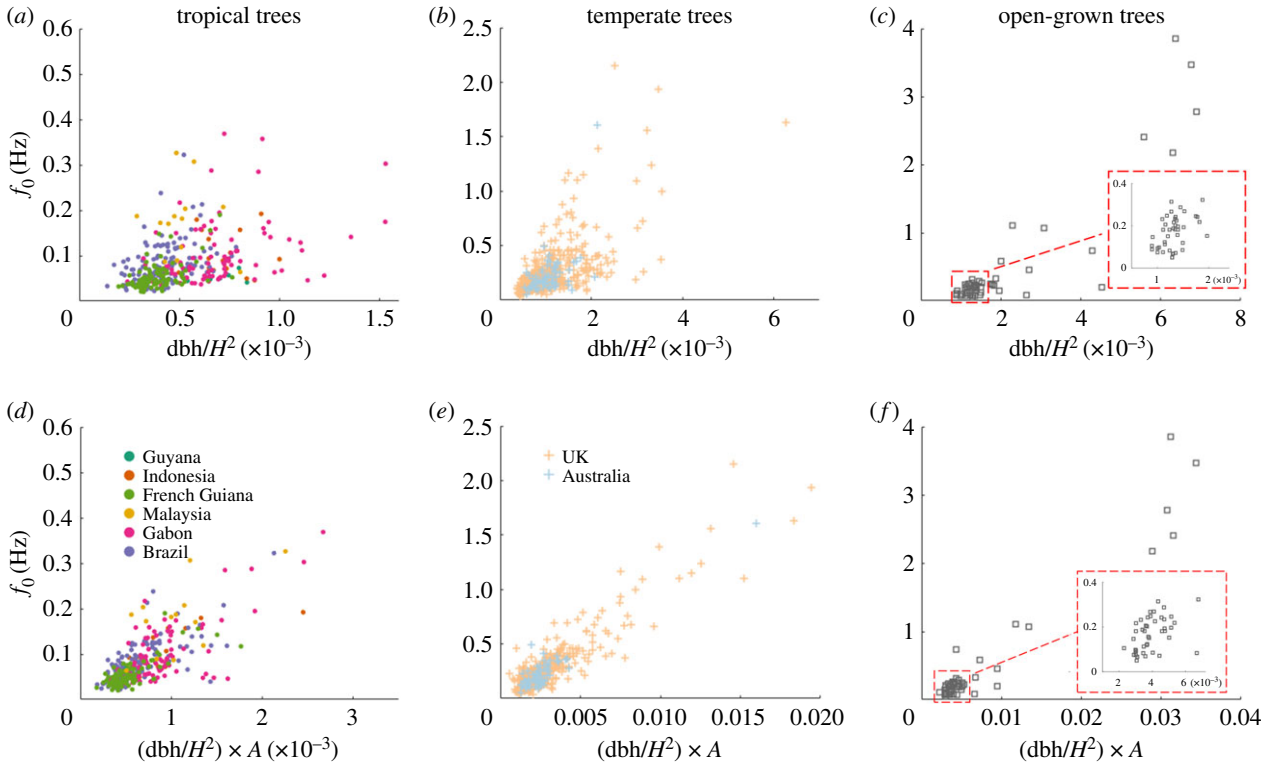

Figure 5. Simulated fundamental frequencies. (*a–c*) Cantilever beam approximation predicting simulated f_0. (*d–f*) Predicting simulated f_0 using architectural information. Here A = (CVR + crown asymmetry + aspect ratio). Panels *a,d* are tropical forest trees, *b,e* are temperate forest trees and *c,f* are open-grown trees. The red-outlined insets in panels *c,f* give a closer view of the data near the origin, these sections correspond to the subsample for which summary statistics are given in parentheses in table 1. Note the difference in *y*-axis ranges.

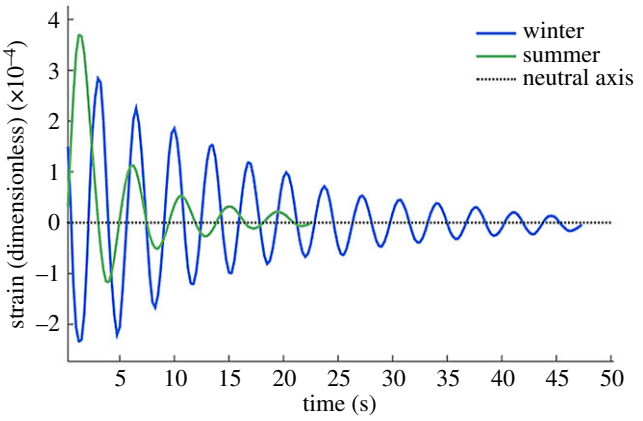

Figure 6. The effect of leaves on tree sway. Summer and winter pull and release test for a single sycamore tree in Wytham Woods, Oxford. (Online version in colour.)

was significant residual variation in f_0. This variation was not explained by material properties for a subset of 40 broadleaf trees. Moreover, our sensitivity analysis (electronic supplementary material, table S3) showed that variations in material properties are unlikely to explain this residual variation in general, since wood density and modulus of elasticity are strongly correlated [42]. Our modelling work shows that tree architectural information can increase the predictability of f_0 by approximately 40% for temperate and tropical forest broadleaf trees.

In deciduous forests, the presence of leaves caused an 18% increase in f_0 and a doubling of damping efficiency, which is similar to previous studies [22,46,47]. This increase in f_0 was due to the weight of the leaves, rather than the increased aerodynamic damping. Additionally, both water uptake and soil state can alter f_0 [22,25]. However, predicting leaf mass or volume of water uptake by the changes they cause in f_0 is difficult, since these changes are highly sensitive to their distribution within the tree.

The swaying behaviour of broadleaf trees in the wind may comprise more than a single significant natural frequency and we defined D_0, the dominance of the fundamental sway mode, to quantify this. D_0 can be thought of as an indication of the tractability of simpler (e.g. modal dynamics) modelling techniques [15] and as a proxy for the efficiency of multiple resonance damping [14]. Despite the fact that three-dimensional tree structure was fully mapped and specified in a virtual environment, we were not able to satisfactorily explain the resulting variation of D_0 using our architectural indices. This result suggests that D_0 is driven by finer scale properties, such as the presence of a single large branch, that are not captured by our tree-level architectural indices [48].

4.3. Implications and future directions

Tall, slender trees tended have lower f_0 and higher D_0, making them simultaneously easier to understand using a simple model [5] as well as potentially more vulnerable to wind damage. These tall trees store the majority of carbon in many tropical forests and have a high conservation value [49]. As a result, improved predictions of the likelihood of wind damage for tall tropical trees would be both tractable and highly valuable.

Overall, we have shown how detailed measurements of tree architecture gives us new insight into the dynamic properties of trees. Our work has quantified the relative importance of tree architectural indices in predicting natural frequencies,

while also highlighting the greater challenge of developing a general model for energy dissipation in complex tree architectures. Our modelling approach, combining TLS data with finite-element analysis, could also be useful for valuable open-grown trees, to inform risk assessments and test proposed interventions in a virtual environment. With TLS-derived tree architectural information now becoming widely available, this is an area ripe for further inquiry.

Data accessibility. All field data collected for this study are available online (dois: 10.5285/533d87d3-48c1-4c6e-9f2f-fda273ab45bc; 657f420e-f956-4c33-b7d6-98c7a18aa07a). Field data from previous studies are available in the original publications. QSMs and software used to convert them to Abaqus input files are available online (http://doi.org/10.5281/zenodo.894543). Architectural indices were extracted in Matlab (https://github.com/TobyDJackson/TreeQSM_Architecture). An updated library for analysing tree structural information is also available in R (https://github.com/ashenkin/treestruct). Scripts used to create figures and run statistical analysis are available from the author on reasonable request.

Authors' contributions. T.J., A.S. and Y.M. wrote the manuscript. J.M., A.B., T.v.E., B.K., D.B. and K.J. provided field data. K.C., N.O., M.D., A.B., P.W., P.R., J.G.T.M., A.L., M.H. and R.C.G. were involved with TLS data collection and processing. A.S., Y.M., T.v.E., K.J., J.S. and T.F. provided valuable feedback and ideas at the early stages of this study.

Competing interests. The authors declare that they have no conflicts of interest.

Funding. This research was supported by an NERC studentship to T.J. (NE/L0021612/1). A.S. and Y.M. are supported by NERC grant no. NE/P012337/1 (to Y.M.) and Y.M. is also supported by the Frank Jackson Foundation. A.L., M.H. and J.G.T. are supported by CIFOR's Global Comparative Study on REDD+, and ERA-GAS NWO-3Dfor-Mod project 5160957540. M.D. was supported in part by NERC NCEO for travel and capital funding for lidar equipment, and NERC Standard grant nos. NE/N00373X/1 and NE/P011780/1. TLS data collection at Wytham Woods was funded through the Metrology for Earth Observation and Climate project (MetEOC-2), grant no. ENV55 within the European Metrology Research Programme (EMRP). The EMRP is jointly funded by the EMRP participating countries within EURAMET and the European Union.

Acknowledgements. We thank partners for supporting TLS data collection in their sites. For Danum Valley in Malaysia, the Sabah Forestry Department and the Sabah Biodiversity Council. For Lopé in Gabon, the Agence National de Parcs du Gabon. For Caxiuanã in Brazil, Museu Paraense Emílio Goeldi. For Wineperu in Guyana, the Guyana Forestry Commission. We also thank D. Culvenor and G. Newnham for supporting the TLS data collection at Rushworth Forest.

References

1. Mayer H. 1987 Wind-induced tree sways. *Trees* **1**, 195–206. (doi:10.1007/BF01816816)
2. Mayhead GJ. 1973 Sway periods of forest trees. *Scottish For.* **27**, 19–23.
3. Kane B, Modarres-Sadeghi Y, James KR, Reiland M. 2014 Effects of crown structure on the sway characteristics of large decurrent trees. *Trees Struct. Funct.* **28**, 151–159. (doi:10.1007/s00468-013-0938-1)
4. Sellier D, Fourcaud T. 2009 Crown structure and wood properties: influence on tree sway and response to high winds. *Am. J. Bot.* **96**, 885–896. (doi:10.3732/ajb.0800226)
5. Pivato D, Dupont S, Brunet Y. 2014 A simple tree swaying model for forest motion in windstorm conditions. *Trees Struct. Funct.* **28**, 281–293. (doi:10.1007/s00468-013-0948-z)
6. Malhi Y, Jackson T, Bentley LP, Lau A, Shenkin A, Herold M, Calders K, Bartholomeus H, Disney MI. 2018 New perspectives on the ecology of tree structure and tree communities through terrestrial laser scanning. *Interface Focus* **8**, 20170052. (doi:10.1098/rsfs.2017.0052)
7. Finnigan J. 2000 Turbulence in plant canopies. *Annu. Rev. Fluid Mech.* **32**, 519–571. (doi:10.1146/annurev.fluid.32.1.519)
8. Gardiner BA. 1992 Mathematical modelling of the static and dynamic characteristics of plantation trees. In *Mathematical modelling of forest ecosystems* (eds J Franke, AE Roeder), pp. 40–61. Frankfurt, Germany: Saunders Verlag.
9. Moore JR, Maguire DA. 2004 Natural sway frequencies and damping ratios of trees: concepts, review and synthesis of previous studies. *Trees Struct. Funct.* **18**, 195–203. (doi:10.1007/s00468-003-0295-6)
10. Peltola H, Gardiner BA, Nicoll CB. 2013 Mechanics of wind damage. In *Living with storm damage to forests: what science can tell us* (eds B Gardiner, A Schuck, M-J Schelhaas, C Orazio, K Blennow, B Nicoll), pp. 31–38. Joensuu, Finland: European Forest Institute.
11. MooreJ, Gardiner B, Sellier D. 2018 Tree mechanics and wind loading. In *Plant biomechanics* (eds A Geitmann, J Gril), pp. 79–106. Cham, Switzerland: Springer International Publishing.
12. Ciftci C, Brena SF, Kane B, Arwade SR. 2013 The effect of crown architecture on dynamic amplification factor of an open-grown sugar maple (*Acer saccharum* L). *Trees Struct. Funct.* **27**, 1175–1189. (doi:10.1007/s00468-013-0867-z)
13. Schindler D, Mohr M. 2018 Non-oscillatory response to wind loading dominates movement of Scots pine trees. *Agric. For. Meteorol.* **250–251**, 209–216. (doi:10.1016/j.agrformet.2017.12.258)
14. Spatz HC, Brüchert F, Pfisterer J. 2007 Multiple resonance damping or how do trees escape dangerously large oscillations? *Am. J. Bot.* **94**, 1603–1611. (doi:10.3732/ajb.94.10.1603)
15. Dupont S, Pivato D, Brunet Y. 2015 Wind damage propagation in forests. *Agric. For. Meteorol.* **214–215**, 243–251. (doi:10.1016/j.agrformet.2015.07.010)
16. Schindler D, Schönborn J, Fugmann H, Mayer H. 2013 Responses of an individual deciduous broadleaved tree to wind excitation. *Agric. For. Meteorol.* **177**, 69–82. (doi:10.1016/j.agrformet.2013.04.001)
17. Spatz H, Theckes B. 2013 Plant science oscillation damping in trees. *Plant Sci.* **207**, 66–71. (doi:10.1016/j.plantsci.2013.02.015)
18. Théckès B, Boutillon X, De Langre E. 2015 On the efficiency and robustness of damping by branching. *J. Sound Vib.* **357**, 35–50. (doi:10.1016/j.jsv.2015.07.018)
19. Moore JR, Gardiner BA, Blackburn GRA, Brickman A, Maguire DA. 2005 An inexpensive instrument to measure the dynamic response of standing trees to wind loading. *Agric. For. Meteorol.* **132**, 78–83. (doi:10.1016/j.agrformet.2005.07.007)
20. Krauss TP, Shure L, Little J. 1994 *Signal processing toolbox for use with MATLAB®: user's guide*. Natick, MA: The MathWorks Inc.
21. Baker CJ. 1997 Measurements of the natural frequencies of trees. *J. Exp. Bot.* **48**, 1125–1132. (doi:10.1093/jxb/48.5.1125)
22. Bunce A, Volin JC, Miller DR, Parent J, Rudnicki M. 2019 Determinants of tree sway frequency in temperate deciduous forests of the Northeast United States. *Agric. For. Meteorol.* **266–267**, 87–96. (doi:10.1016/J.AGRFORMET.2018.11.020)
23. James KR, Haritos N, Ades PK. 2006 Mechanical stability of trees under dynamic loads. *Am. J. Bot.* **93**, 1522–1530. (doi:10.3732/ajb.93.10.1522)
24. van Emmerik T, Steele-Dunne S, Guerin M, Gentine P, Oliveira R, Hut R, Selker J, Wagner J, van de Giesen N. 2018 Tree *Sway Time Series* of 7 Amazon *Tree Species* (July 2015–May 2016). *Front. Earth Sci.* **6**, 221. (doi:10.3389/feart.2018.00221)
25. Van Emmerik T, Steele-Dunne S, Hut R, Gentine P, Guerin M, Oliveira RS, Wagner J, Selker J, Van De Giesen N. 2017 Measuring tree properties and responses using low-cost accelerometers. *Sensors* (*Switzerland*) **17**, 1098. (doi:10.3390/s17051098)
26. Åkerblom M. 2017 Inversetampere/Treeqsm: initial release. Zenodo. (doi:10.5281/zenodo.844626)
27. Calders K, Origo N, Burt A, Disney M, Nightingale J, Raumonen P, Åkerblom M, Malhi Y, Lewis P. 2018 Realistic forest stand reconstruction from terrestrial LiDAR for radiative transfer modelling. *Remote Sens.* **10**, 933. (doi:10.3390/rs10060933)

28. Calders K *et al.* 2015 Nondestructive estimates of above-ground biomass using terrestrial laser scanning. *Methods Ecol. Evol.* **6**, 198–208. (doi:10.1111/2041-210X.12301)
29. Disney MI, Boni Vicari M, Burt A, Calders K, Lewis SL, Raumonen P, Wilkes P. 2018 Weighing trees with lasers: advances, challenges and opportunities. *Interface Focus* **8**, 20170048. (doi:10.1098/rsfs.2017.0048)
30. Gonzalez de Tanago Menaca J *et al.* 2017 Estimation of above-ground biomass of large tropical trees with terrestrial LiDAR. *Methods Ecol. Evol.* **9**, 223–234. (doi:10.1111/2041-210X.12904)
31. Lau A, Bentley LP, Martius C, Shenkin A, Bartholomeus H, Raumonen P, Malhi Y, Jackson T, Herold M. 2018 Quantifying branch architecture of tropical trees using terrestrial LiDAR and 3D modelling. *Trees Struct. Funct.* **32**, 1219–1231. (doi:10.1007/s00468-018-1704-1)
32. Wilkes P, Disney M, Boni Vicari M, Calders K, Burt A. 2018 Estimating urban above ground biomass with multi-scale LiDAR. *Carbon Balance Manag.* **13**, 10. (doi:10.1186/s13021-018-0098-0)
33. Wilkes P, Lau A, Disney M, Calders K, Burt A, Gonzalez de Tanago J, Bartholomeus H, Brede B, Herold M. 2017. Data acquisition considerations for terrestrial laser scanning of forest plots. *Remote Sens. Environ.* **196**, 140–153. doi:10.1016/j.rse.2017.04.030
34. Bentley LP, Stegen JC, Savage VM, Smith DD, von Allmen EI, Sperry JS, Reich PB, Enquist BJ. 2013 An empirical assessment of tree branching networks and implications for plant allometric scaling models. *Ecol. Lett.* **16**, 1069–1078. (doi:10.1111/ele.12127)
35. Savage VM, Bentley LP, Enquist BJ, Sperry JS, Smith DD, Reich PB, von Allmen EI. 2010 Hydraulic trade-offs and space filling enable better predictions of vascular structure and function in plants. *Proc. Natl Acad. Sci. USA* **107**, 22 722–22 727. (doi:10.1073/pnas.1012194108)
36. Åkerblom M, Raumonen P, Mäkipää R, Kaasalainen M. 2017 Automatic tree species recognition with quantitative structure models. *Remote Sens. Environ.* **191**, 1–12. (doi:10.1016/j.rse.2016.12.002)
37. Moore JR, Maguire DA. 2008 Simulating the dynamic behavior of Douglas-fir trees under applied loads by the finite element method. *Tree Physiol.* **28**, 75–83. (doi:10.1093/treephys/28.1.75)
38. Sellier D, Brunet Y, Fourcaud T. 2008 A numerical model of tree aerodynamic response to a turbulent airflow. *Forestry* **81**, 279–297. (doi:10.1093/forestry/cpn024)
39. Simulia Software Company. 2017 Abaqus Theory Guide Abacus 6.41. 2014.
40. Viberg M. 1995 Subspace-based methods for the identification of linear time-invariant systems. *Automatica* **31**, 1835–1851. (doi:10.1016/0005-1098(95)00107-5)
41. Jackson T *et al.* 2019 Finite element analysis of trees in the wind based on terrestrial laser scanning data. *Agric. For. Meteorol.* **265**, 137–144. (doi:10.1016/j.agrformet.2018.11.014)
42. Niklas KJ, Spatz HC. 2010 Worldwide correlations of mechanical properties and green wood density. *Am. J. Bot.* **97**, 1587–1594. (doi:10.3732/ajb.1000150)
43. Espírito-Santo FDB *et al.* 2014 Size and frequency of natural forest disturbances and the Amazon forest carbon balance. *Nat. Commun.* **5**, 3434. (doi:10.1038/ncomms4434)
44. Magnabosco Marra D *et al.* 2018 Windthrows control biomass patterns and functional composition of Amazon forests. *Glob. Chang. Biol.* **24**, 5867–5881. doi:10.1111/gcb.14457)
45. Silvério DV, Brando PM, Bustamante MMC, Putz FE, Marra DM, Levick SR, Trumbore SE. 2018 Fire, fragmentation, and windstorms: a recipe for tropical forest degradation. *J. Ecol.* **107**, 656–667. (doi:10.1111/1365-2745.13076)
46. Kane B, James KR. 2011 Dynamic properties of open-grown deciduous trees. *Can. J. For. Res.* **41**, 321–330. (doi:10.1139/X10-211)
47. Reiland M, Kane B, Modarres-Sadeghi Y, Ryan HDP. 2015 The effect of cables and leaves on the dynamic properties of red oak (*Quercus rubra*) with co-dominant stems. *Urban For. Urban Green.* **14**, 844–850. (doi:10.1016/j.ufug.2015.08.010)
48. Sellier D, Fourcaud T. 2005 A mechanical analysis of the relationship between free oscillations of *Pinus pinaster* Ait. saplings and their aerial architecture. *J. Exp. Bot.* **56**, 1563–1573. (doi:10.1093/jxb/eri151)
49. Slik JWF *et al.* 2013 Large trees drive forest aboveground biomass variation in moist lowland forests across the tropics. *Glob. Ecol. Biogeogr.* **22**, 1261–1271. (doi:10.1111/geb.12092)